Some proposal for modelling the main components of a drone-mounted vineyard pesticide sprayer circuit

ISSN 1590-8844
Vol. 25 No. 02
2024

International Journal of Mechanics and Control

Editor: Andrea Manuello Bertetto

Scopus Indexed Journal

Reference Journal of IFToMM Italy
International Federation for the Promotion
of Mechanism and Machine Science

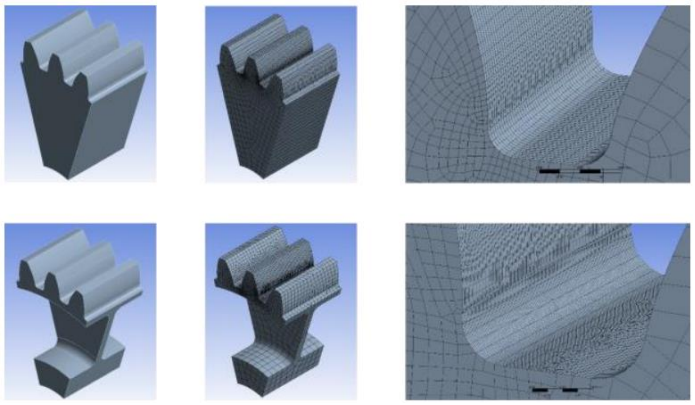

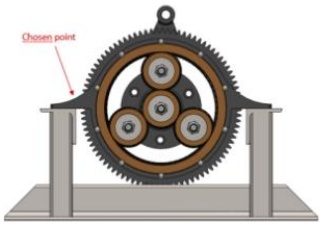

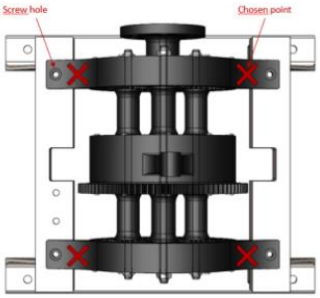

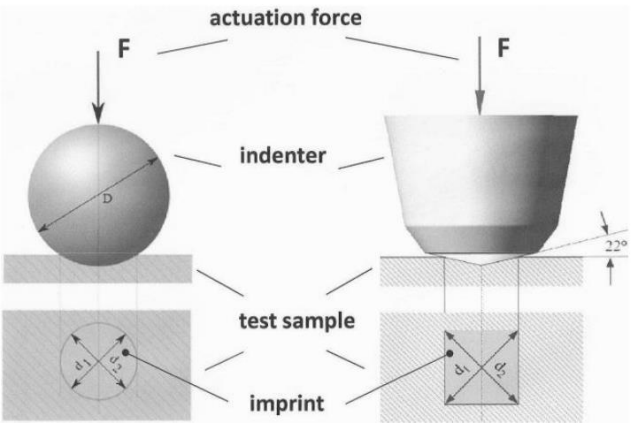

Published by ASTRA M B S.R.L.
Via Febo, 22 – 10133 – Torino (Italy)

International Journal of Mechanics and Control

Associate Editors

Published by ASTRA M B S.R.L. – Torino – Italy E.C.

Official Torino Italy Court Registration
n. 5390, 5th May 2000

Deposito presso il Tribunale di Torino
n. 5390 del 5 maggio 2000

Direttore responsabile:
Andrea Manuello Bertetto

ISSN 1590-8844
International Journal of Mechanics and Control, Vol. 25, No. 02, 2024

https://doi.org/10.69076/jomac.2024.0029

SOME PROPOSALS FOR MODELLING THE MAIN COMPONENTS OF A DRONE-MOUNTED VINEYARD PESTICIDE SPRAYER CIRCUIT

T. Raparelli* N. Filippi** G. Eula*

* Department of Mechanical and Aerospace Engineering, Politecnico di Torino, Torino, Italy

** Agrati Group CVB Srl, Tronzano Vercellese (VC), Italy

ABSTRACT

Using drones in agriculture often makes it possible to change or to improve operations such as pesticide spraying. This paper presents an analysis of several commercial spray nozzles conducted in order to design a drone-mounted vineyard spraying circuit. In particular, the paper illustrates several models of these nozzles developed on a commercial software platform. These models were used to analyze the behavior of different nozzles on the basis of catalog data, thus making it possible to design and optimize the spraying circuit before components are purchased. These models were investigated in different ways, and the preliminary results obtained were compared with those from experimental tests. The comparison yielded good results and demonstrates the models' reliability. In addition, the commercial software platform was used to construct several models of the spraying circuit, investigating various possible operating and failure scenarios.

Keywords: Drone in vineyard, pesticide spraying, vineyard treatments, soil pollution

1 INTRODUCTION

Vineyards are subject to many types of diseases, which can cause losses of up to 35%. Consequently, the vines must be sprayed with plant protection products 7 to 10 times per summer season. [1-6] When conventional spraying methods are used, a large quantity of product can miss the target and fall on the ground if the sprayers are not properly adjusted.
In some cases, as much as 30-50% of the liquid may be wasted. This liquid dispersed in the soil results in less effective protection for the vineyard and pollutes the environment, harming plant and animal life. Currently, viticulture's goal is to produce with less and reduce environmental impact. Agriculture 4.0 seeks to use technologically advanced systems to optimize resources and reduce the use of products that can create environmental pollution.
From this standpoint, developing innovative pesticide sprayer systems can be important for the environment and for ensuring that products are correctly used in order to improve product deposition, reduce spray drift, waste and costs, and optimize crop protection. Drones are already employed in agriculture, above all to collect data in the field. For example, drones equipped with multispectral cameras have been used to create vigor maps. [2] Drones can benefit crop spraying in several ways: they can reach otherwise inaccessible areas, spray more accurately, are unaffected by soil condition, do not crush crops, reduce operator exposure to dangerous substances, and do not cause soil compaction. They are already used for weed control and for various purposes in cereal crops. In the literature, several studies [3] have analyzed the performance of agricultural sprayer circuits. In particular, the effect of nozzle orientation on droplet size and velocity has been investigated. The main factors at work in this connection were found to be the distance between the spray nozzles and the crop, the orientation of each nozzle, and the effect of gravity. Such studies improve our understanding of spraying conditions in order to optimize droplet distribution on the crop and prevent spray drift [7-15]. In general, the main parameters to be taken into consideration to optimize spraying performance are nozzle type, droplet size, flight height and drone speed [16-23]. Scenarios involving possible failure conditions for the drone-mounted sprayer circuit can be investigated to optimize circuit design and nozzle selection.

Contact author: Gabriella Eula[1]

[1] Dept. of Mechanical and Aerospace Eng., Politecnico di Torino, Torino, Italy
E-mail: gabriella.eula@polito.it

In earlier work, the authors carried out research on spraying systems for use in greenhouses [20-23] and in vineyards [24-26]. These studies were useful in developing nozzle testing procedures, analyzing test results, and designing innovative prototypes capable of improving crop spraying operations. The present study addresses the problems arising during aerial spraying to determine whether UAVs are also suitable for vineyard applications, starting from the analysis and the design of the sprayer circuit. To this end, a hydraulic circuit was designed using commercial components that made it possible to analyze circuit parameters in a software environment, obtaining important information on pesticide spraying performance. Previous studies by the authors addressed the factors having the greatest influence on droplet deposition on the leaves in conventional and drone-mounted spray systems [26, 27]. As a preliminary step in hydraulic circuit design, the problems that can arise using a drone were identified via a review of the literature on airborne spray drift and the downwash flow generated by rotors, which can have negative effects on deposition. It was found that these phenomena are heavily influenced by droplet size. Drift is also a major problem in conventional agriculture, and attempts have been made to mitigate its effects by adopting appropriate precautions for spray equipment and the surrounding environment. [3, 4].

Drift when using drones to spray crops such as rice was investigated in [5], finding that droplet $D_{v0.5}$ should not be less than 160 μm to minimize drift [4, 7]. $D_{v0.5}$ is the VMD (Volume Median Diameter), i.e., the droplet diameter where 50% of the spray volume consists of droplets with a diameter less than this value, and 50% consists of larger droplets. The second problem encountered with aerial systems is related to the air currents generated by the rotor blades. These flows are orderly in hovering conditions [6], while in dynamic flight vortices develop and disturb an increasingly large area as the forward speed of the drone increases. At high speeds, horseshoe-shaped vortices form which can increase drift potential and lead to deposition problems [7]. For the drone-mounted sprayer circuit, the authors analyzed various types of commercial nozzles operating at different flow rates and generating droplets of different sizes. Each nozzle model has different characteristics and is used in agriculture for different applications. Nozzle behavior was characterized by calculating the discharge coefficients whereby liquid flow is obtained as a function of supply pressure. These coefficients were then used to model the hydraulic circuit using a simulation software platform. In this part of the study, the coefficients and nozzle representation methods contemplated by the software platform were evaluated with the nozzle flowrates stated by the manufacturer. First, the main circuit was set up with the Simcenter Amesim software platform and various coefficients from the nozzle catalog were used in turn in an attempt to improve nozzle modeling. As the simulated flowrates for all operating conditions differed from those stated by the manufacturer when coefficients from the nozzle catalog were used, the authors constructed the entire nozzle characteristic curve (flowrate versus supply pressure) and introduced it in the modeled circuit, obtaining satisfactory simulation results.

The authors used a second method to simulate the nozzles with the platform starting from catalog data, and the two nozzle modeling techniques were compared. The reliability of the nozzle models was then checked by comparing both methods with the results of experimental tests. After selecting appropriate components and building the complete circuit on the Simcenter Amesim platform, the authors evaluated circuit spraying performance. This paper thus presents a method for analyzing droplet generation in several specific models and simulations, investigating the influence of the operating parameters in various configurations and scenarios. The following sections will illustrate nozzle and pump selection for these applications, the design of several simulation circuits on the software platform, the possible scenarios that can be analyzing with them, and the results obtained using these models.

2 MATERIALS AND METHODS

The modern agricultural drones currently on the market were designed specifically for use on flat field crops such as cereals. As using drones for pesticide spraying in vineyards is innovative, it is necessary to examine the problems that can arise in this application. The drone considered in this study was a DJI AGRAS MG-1 octocopter with a maximum operating speed of 8 m/s, K_v rating 130 rpm/V (that is the ratio between the velocity and the Volt required) and 10 kg payload. The drone was equipped with a sprayer circuit as shown in the block diagram in Figure 1.

The hydraulic circuit features a 10 l capacity tank, a diaphragm pump, rubber connecting hoses, quick-connect couplings, nozzles and the associated nozzle holders, and sensors for the circuit operating parameters.

The type and the number of the circuit components are important in order to reduce the load on the drone. In the future, after a proper experimentation, an anti-sloshing tank could be provided in this circuit, allowing not to use the pump. In connection with the following analyses, it should be borne in mind that 1 bar = 10^5 Pa; 1 l = 10^{-3} m^3; 1 min = 60 s.

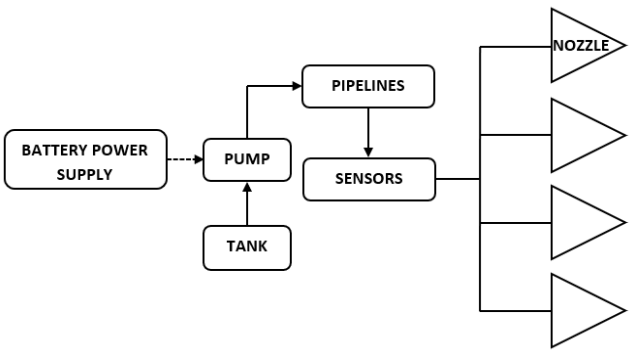

Figure 1 Sprayer circuit block diagram.

3 VINEYARD ANALYSIS

Unlike crops such as rice, grape vines are planted in rows and trained vertically, calling for different drone flight strategies. Accordingly, several key vineyard dimensions were taken into consideration in order to simulate nozzle position relative to the crop during drone flight. The differences between some common vineyard types of vineyards were investigated in order to obtain general information for use in simulating actual spraying conditions for different grape varieties and vineyard arrangements found in the Biella, Cuneo and Vercelli areas of Italy's Piemonte region. Figure 2a is a simulated view of the drone flying over an actual vineyard producing Gattinara DOCG wine from Nebbiolo grapes in the Vercelli area of northern Piemonte. Here the vineyard dimensions were similar to those of the "Antica Meridiana Relais-Art" vineyard (Cuneo, Italy). Figure 2b shows the authors' CAD model [25] based on the dimensions kindly indicated by the M. Martinelli family, owners of the "Antica Meridiana Relais-Art" Dolcetto vineyard in Vicoforte, Cuneo, Italy (Figure 2b).

Figure 2a View of drone flying over the Gattinara vineyard.

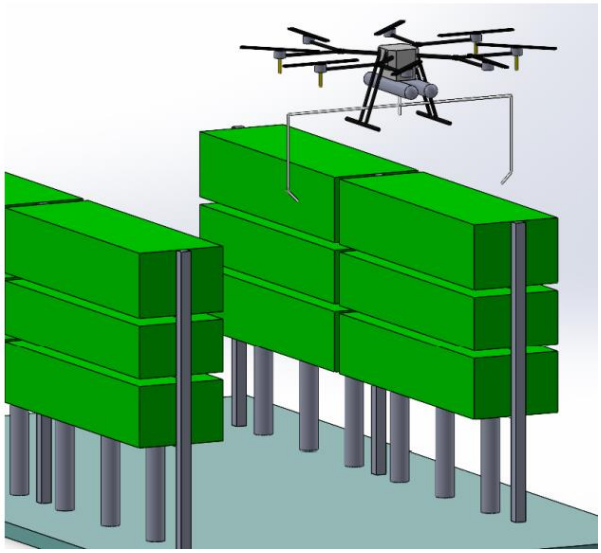

Figure 2b CAD model of drone flight in a vineyard (based on the dimensions of the "Antica Meridiana Relais-Art" vineyard).

To gain further information about vineyard dimensions, additional measurements were made of the guyot-pruned Erbaluce vines (Figures 3a and b) in the Azienda Agricola Pastoris vineyard (Viverone – Biella – Italy). Here, canopy height *h* is 1.9-2.2 m and row spacing *b* is 2.0-2.3 m.

Flight attitude and nozzle orientation must be such as to avoid two potential problems arising in the vineyard: sedimenting drift deposits on the ground, and insufficient deposition on the bottom of the canopy. Three flight paths were considered: drone centered between rows, drone flying across rows, drone above the row. The first flight path can be adopted when the distance between the rows is small, as two rows can be sprayed at the same time, but care must be taken as part of the spray can fall on the ground.

Figure 3a An example of some dimensions in the Pastoris vineyard.

Figure 3b Some additional dimensions in the Pastoris vineyard.

The second flight path can be used when crosswinds are likely, but here again attention to spray efficacy is required. The third flight path, which is probably the best, can be adopted by reducing flight height as much as possible and checking that the leaves at the bottom of the canopy are also sprayed effectively. In all cases, field tests with droplet collectors as described in [6] must be carried out to optimize flight parameters. In this connection, investigations of the effect of drone flight and rotors on the spray jet yielded interesting findings [27, 28]. Droplet drift and rotor downwash were also considered [2, 4, 9, 10, 12, 14, 17, 27, 28].

4 PRELIMINARY NOZZLE SELECTION

Sprayer nozzles must be selected on the basis of the drone flight path and the need to generate droplets of a size suitable for spraying in the open field (diameters from 200 to 400 μm). The flight path must be considered in determining the number and layout of the nozzles carried under the drone, to avoid droplet drift caused by rotor spin and drone forward movement. In the example shown in Figures 4a-c, vineyard dimensions are those indicated for the Martinelli vineyard. The authors investigated several nozzle layouts, graphically simulating the nozzle jets as shown in the figures in order to optimize the sprayer circuit configuration and distribute pesticide on the entire crop with a minimum number of drone passes. Figures 4a-c show possible configurations analysed using, for example, the ASJ Spray-jet HCF80015 full cone jet nozzle (hereafter designated as H).

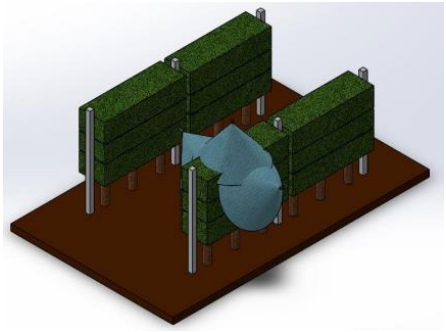

Figure 4a Some tests with full cone jet nozzles in the first vineyard examined here.

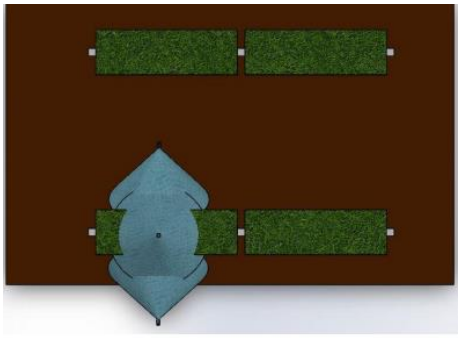

Figure 4b A top view of full cone jet nozzles in the first vineyard examined here.

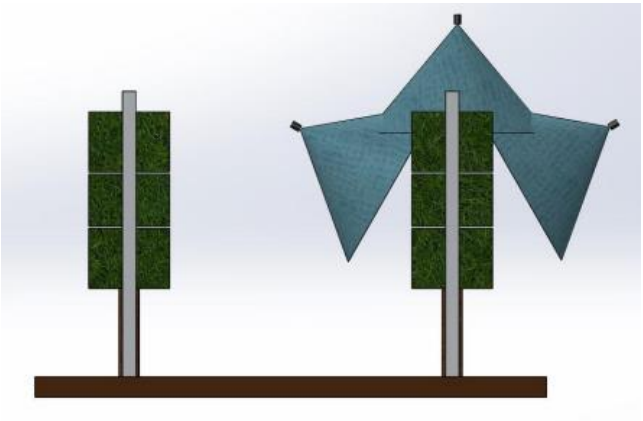

Figure 4c A side view of full cone jet nozzles in the first vineyard examined here.

The configuration uses three full cone nozzles capable of generating 177 to 218 micron droplets at a pressure of 2-3 bar (1 bar = 10^5 Pa) and a cone angle from 80° to 110° arranged in order to cover the entire crop from above and along its height.

The goal is to reach as much of the crop as possible with a minimum number of nozzles and drone passes, in order to minimize drone load and optimize pesticide consumption. Different nozzle models can have different flowrates and generate droplets of different diameters. Specifically, the nozzles shown in Table I were considered, viz., TXA, AITX and XR from TeeJet Technologies® (USA) [29]; HCF80015 and LDC11001 from ASJ Spray-jet, an ARAG Group Company (Italy) [30].

For the purposes of this study, nozzles were designated as follows: A = TXA800050VK (TeeJet) B = TXA800067VK (TeeJet), C = TXA8001VK (TeeJet), D = TXA80015VK (TeeJet), E = AITX8001VK (TeeJet), F = XR8001 (TeeJet), G = HCA8001 (ASJ Spray-jet), H = HCF80015 (ASJ Spray-jet), I = HC16001 (ASJ Spray-jet), L = HCI80015 (ASJ Spray-jet), M = LDC11001 (ASJ Spray-jet), N = WRC110015 (ASJ Spray-jet), O = AFC11001 (ASJ Spray-jet). It should be emphasized that this was a preliminary selection based on the nozzles' ability to generate droplets with appropriate diameters for this application, spray angle, supply pressure and flowrate. The spray angle for nozzles A, B, C, D refers to a supply pressure of 7 bar (1 bar = 10^5 Pa), while no information is available for nozzle E. The TXA cone nozzles (here designated as A, B, C, D) were selected inasmuch as the manufacturer's catalog indicates that they are suitable for vineyard applications, while the AITX nozzle (here designated as E) was selected because its air induction design reduces drift by generating larger droplets. The XR nozzle (here designated as F) was selected because it operates at lower supply pressures with the same flowrate, producing larger droplets than the TXA nozzles. The TXA and XR nozzles are designed for multiple applications, while the air induction AITX nozzle provides good drift control. For each of these nozzles, various spraying scenarios were simulated on the Simcenter Amesim platform to study the circuit parameters.

Table I – Nozzle models and main characteristics

Nozzle name	Type	Range (bar)	Angle (degree)	D 0,5 (μm)
A	Cone	3-20	80	107
B	Cone	3-20	80	115
C	Cone	3-20	80	132
D	cone	3-20	80	157
E	Air induction cone	4-20	.	556
F	Flat	1-4	80-110	189
G	Hollow cone	5-15	80	404-502
H	Full cone	2-6	80	106-235
I	Hollow cone	5-15	60	61-105
L	Hollow cone	5-15	80	106-235
M	Antidrift flat jet	2-4	110	236-340
N	Fan jet	2-3	110	106-235
O	Antidrift fan jet	2.5-5	110	341-403

In selecting nozzles, particular attention was paid to nozzle size to ensure tank emptying times that optimize drone battery life. Several diaphragm pumps were modeled in the circuit to determined their performance in combination with each nozzle type. In simulating the circuit, the diaphragm pumps' Q-P curves implemented on the software platform were obtained from [11] and by contacting the manufacturer. Other useful information about suitable pumps for this application was obtained from [11] and used in the models. The SEAFLO pump (SEAFLO North America, South Bend, USA) was selected because it features PWM control. As can be seen from Table II and Figure 5, the pumps differ in their characteristics and performance. As pumps must be mounted on the drone, weight was a major consideration in selection.

Table II – Pump models

Commercial designation	Pump	Power supply (V)	Mass (kg)
JMRRC BPP-25	P1	22-25	0.30
Propump	P2	12	1.00
Singflo FLO-2203a	P3	12	0.67
Seaflo 22 series	P4	12	1.10
Seaflo 22 series	P5	24	1.10

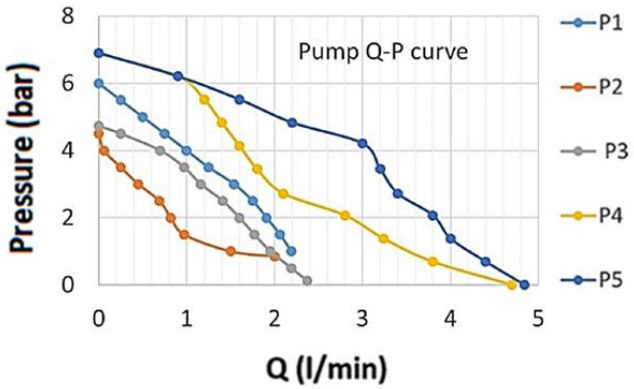

Figure 5 Pump characteristic curves (1 bar = 10^5 Pa).

5 NOZZLE MODELLING WITH THE SOFTWARE PLATFORM

Droplet generation was investigated in order to model the pesticide sprayer circuit, nozzles and nozzle behavior realistically. Droplet formation mechanisms and the parameters that influence this process have been investigated in the literature [10,11]. In open field spraying operations, where wind and other disturbances may be encountered, it is advisable to choose nozzles that generate droplets of the correct size to reduce airborne drift and the effects of rotor downwash. For the application examined here, optimum droplet diameter for preventing wind drift and run-off from the leaves is from 200 to 400 μm. The main difference between the selected nozzles is that type F is a flat nozzle, while types A, B, C, D and E are cone nozzles. The first type is more suitable for use on crops such as cereals, while the other nozzles are used in orchards and vineyards. A flat nozzle produces a long narrow jet, while a full cone nozzle produces a conical spray in a circular or oval pattern. In flat nozzles, the liquid forms a fan shape as it leaves the nozzle orifice, and the droplets cover a rectangular spray pattern, while the cone nozzles considered here feature a swirl chamber which imparts rotary motion to the liquid. This produces a conical spray at the outlet orifice to cover a circular area. The main difference between types A, B, C and D and type E is that the latter has a hole in the nozzle body whereby air is drawn in through the Venturi effect [10] to produce larger air-filled droplets that are less subject to drift. As a fundamental principle of operation, a pressure gradient causes the liquid to flow into the nozzle and then be expelled and atomized. When the liquid sheet reaches the outlet, the instabilities that are created will cause a primary breakup into droplets, followed by a secondary breakup on the part of the larger droplets [8]. In fact, unstable waves are generated when the liquid issues from the nozzle as a result of the cohesive forces and destructive forces due to surface tension and the relative velocity of liquid and air.

If operating conditions are favorable, these waves propagate and break up the jet. The liquid's velocity is very important in this process: the higher the velocity, the greater the impact of aerodynamic effects on increasing jet

instability will be. The type F nozzle was also considered, even if it is not expressly designed for vineyard applications, because it operates with lower supply pressures and generates larger droplets than cone nozzles for any given flowrate.

5.1 THE FIRST PROPOSED NOZZLE MODELLING TECHNIQUE

As the goal is to minimize pesticide use and in view of the fact that the drone dimensions are such that a limited amount of liquid can be carried, it is essential to know the flowrate of the liquid in the circuit at any given time according to supply conditions. To this end, mathematical relationships must be found which, once nozzle geometry is known, can be used to calculate a coefficient linking supply pressure with the flow of liquid in the nozzle. This coefficient is known as the discharge coefficient, and is represents the ratio of the actual flowrate of liquid discharged from the nozzle to the rate that would be theoretically possible. It depends on the nozzle's outlet orifice area and internal geometry. These relationships can be very complicated, and in the case of cone nozzles must take the internal geometry of the swirl chamber into account. The following formula is an example of the mathematical relationships used to calculate the C_D coefficient [8]:

$$C_D = 0.45\left(\frac{d_0\rho_L U}{\mu_L}\right)^{-0.02}\left(\frac{l_0}{d_0}\right)^{-0.03}\left(\frac{L_s}{D_s}\right)^{0.05}\left(\frac{A_p}{D_s d_0}\right)^{0.52}\left(\frac{D_s}{d_0}\right)^{0.23} \quad (1)$$

where: d_0 orifice diameter (m), ρ_L liquid kinematic viscosity (m^2/s), U resultant velocity in orifice (m/s), μ_L liquid dynamic viscosity (kg/ms), l_0 orifice length (m), L_S length of parallel portion of swirl chamber (m), D_S swirl chamber diameter (m), A_p total inlet port area (m^2).

However, due to the complexity of the phenomenon, the simplifications introduced to obtain this formula are too large and the results obtained differ from the experimental ones. In fact, to obtain relationships such as (1), the structure of the vortex generation chamber in the nozzle is simplified, neglecting the friction effects in order to obtain simplified mathematical relationships that can be used without calculation software. As mathematical relationships such as (1) have many limitations because of their initial hypotheses and simplifications, the results they yield are not always satisfactory.Consequently, the C_D coefficient must be calculated from the flowrates indicated versus supply pressure in the nozzle catalog. Once the flowrate through the nozzle as a function of supply pressure and orifice size is known, more precise coefficients can be determined [9]. With the method illustrated in [9] and the data provided in the TeeJet Technologies catalog [10], the various discharge coefficients whereby flowrate can be calculated from the following relationship:

$$Q = C_V\sqrt{2\frac{\Delta p}{\rho_l}}C_A A \quad (2)$$

Here, A is the nozzle's outlet section (m^2), Δp is the total pressure drop (Pa), ρ_l is the liquid density (kg/m^3) and $C_D = C_V C_A$ where C_A is a corrective coefficient for the orifice area and takes vena contracta formation into account.

Using the data provided by the nozzle manufacturer, and in particular the outlet orifice diameter and the nozzle flowrate at different supply pressures, formula (2) gives the coefficients of each nozzle as a function of supply pressure. For example, coefficient C_D of the type B nozzle, with an outlet orifice diameter d_0 = 1,04 mm, in the recommended supply pressure range of use R1: 3-20 bar (1 bar = 10^5 Pa) has range of values R2: 0,26 to 0,20.

As can be seen from the R2 range, the discharge coefficient varies as a function of supply pressure. Due to the nozzle's internal geometry and the vena contracta, the coefficients in this range are also very low compared with 0.611 as normally used for turbulent orifice flow [9]. Because of this discharge coefficient variability R2, the data obtained in the first simulations performed by entering a certain coefficient in the drone circuit simulation software differed from the data obtained experimentally by the nozzle manufacturer. The simulation platform can represent nozzle behavior using different methods that entail entering different input data.

Accordingly, considerable care was taken in this step, since the nozzle and the pump are the most important components in the circuit. Several tests were carried out by building a main circuit on the software platform to determine the best method of representing the nozzle. The first tests were carried out using the C_D coefficients calculated for each nozzle to define its behavior and find the liquid flowrate as a function of supply pressure. To take this coefficient's variability into account, tests carried out on the Simecenter Amesim platform used both the maximum value of the coefficient C_{Dmax} and the mean value C_{Dmean} for each nozzle. As can be seen from the comparison of simulated data and the experimental data supplied by the manufacturer shown in Figure 6, the flowrate differs from that declared by the manufacturer when either the maximum discharge coefficient C_{Dmax} or the mean value C_{Dmean} are used. With C_{Dmax} the difference between the actual flowrate calculated experimentally by the manufacturer and the flowrate calculated by the simulation software is especially marked as pressure increases.

To represent nozzle behavior during spraying realistically, the authors' method of entering the nozzle characteristic directly in the software is thus appropriate. The missing points on the flow curve are automatically filled in by the simulation software through linear or cubic interpolation.

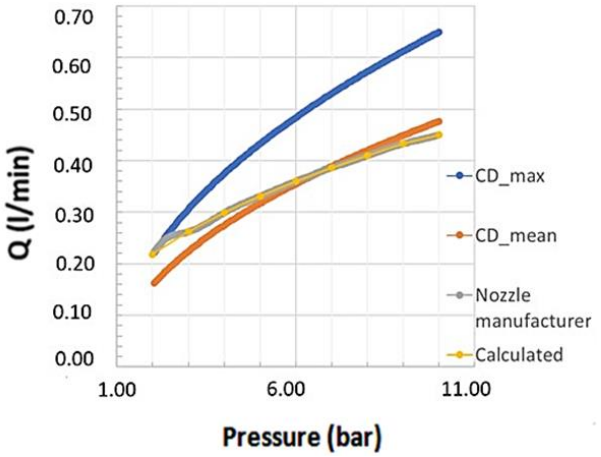

Figure 6 Liquid flowrate for type B nozzle using various methods to model nozzle behavior (1 bar = 10^5 Pa).

This section illustrates the authors' preliminary technique for simulating nozzle behavior in order to construct a model approximating to each nozzle's operation. It is very important that simulations be as close as possible to actual nozzle behavior, as the flowrate provided by the circuit must be accurately adjusted to optimize the pesticide spraying process.

6 MODELS OF THE PESTICIDE SPRAYER CIRCUITS CONSTRUCTED WITH THE FIRST NOZZLE MODELLING TECHNIQUE

Examples of circuits developed on the software platform with nozzles modeled using the first technique are presented below. To test hydraulic circuit performance and parameters during spraying, several circuits with the same characteristics as the one designed, and equipped with all components, were constructed on the simulation platform.
A few preliminary circuits were first set up to determine how best to model the components (pump, nozzle, valve, pipe, sensors, etc.). Subsequently, the authors set up: 1) a circuit to test the performance of the selected nozzles and pumps; 2) a circuit to test potential failure scenarios; 3) a circuit with multiple pumps to test circuit performance if two pumps are used; 4) a circuit including a valve for regulating circuit flowrate, in order to evaluate whether such an application is advantageous; 5) a circuit with a PID-controlled flowrate valve; and 6) a circuit with a pressure reducer controlled in such a way as to maintain constant circuit pressure. Here, only the more significant circuits are presented, viz., circuit 1 with the selected pumps and nozzles, and circuit 2 for potential failure scenarios. Circuits 1 and 2 are equipped with different types of sensor. For circuit 1, all pumps and all nozzles presented here were investigated, while nozzle B and pump P5 were used in circuit 2. As shown in Figure 7, circuit 1 consists of a diaphragm pump, pressure and flow sensors, lengths of flexible hose connected by commercial fittings, and the four nozzles with nozzle holders. Several types of quick-connect couplings and threaded connections were used in the circuits. The circuits also include the pump tank (T); the pump with motor and control signal (MOT and V); various connections (LF, QSL-8, TF, YF); flowrate sensors (S); instantaneous pressure sensors (P); nozzle holder (NH); nozzles (N) with outlet orifice (1 bar); circuit branch designation (L left, R right); flowmeter (F) for measuring flowrate in the left and right branches; piloted nozzle (PT) for simulating a variation in tubing section. In particular, circuit 1 (Figure 7) has two blocks of sensors: one mounted on the pump delivery and designated with the letter S which has three sensors and is used to monitor pump performance, and a second block mounted on a branch of the circuit used to monitor the spray conditions of the single nozzle. The three sensors of the block designated as S measure liquid pressure, instantaneous flowrate, and the volume of liquid delivered by the circuit as a function of time. The connecting lines consist of $8*10^{-3}$ m TPE flexible tubing as commonly used in pneumatics, and can be rapidly assembled through quick-connect couplings.

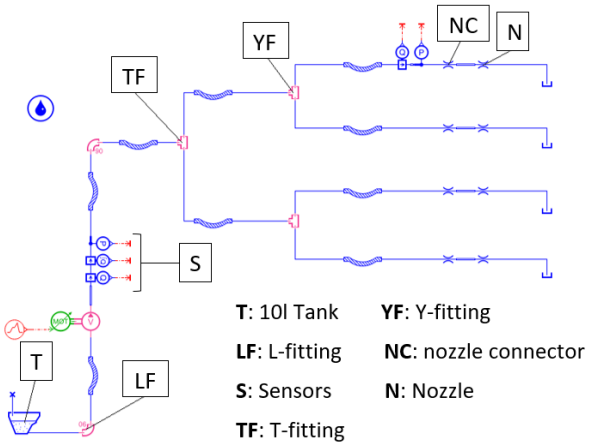

Figure 7 Circuit 1 simulating different nozzles and pumps.

This circuit made it possible to evaluate the performance provided by the selected commercial pumps coupled to the three nozzle models. For the simulations of circuit 1, the focus was on the performance and parameters provided by each pump and nozzles A, B, C, D, E, and F in all possible pump-nozzle configurations. As each nozzle requires a specific minimum pressure to operate correctly, it is important at this stage to check that the selected pump is able to guarantee this pressure. If it cannot, the nozzle will malfunction and the spray droplets will not be of the size declared in the manufacturer's catalog. As nozzle F requires a supply pressure ranging from 1 to 4 bar, a strong pump is not required to reach the minimum circuit operating pressure in the circuit. This is not the case with nozzles A, B, C, D and E, which must be supplied at 3 and 4 bar to operate correctly. For simple cone and air induction cone nozzles, on the other hand, problems arise because the former require a minimum supply pressure of $3*10^5$ Pa while the latter require $4*10^5$ Pa [10]. These values cannot

be reached in the circuit with some of the selected pumps. Table III shows the supply pressures reached upstream of each nozzle with the various pumps installed in the circuit. Only pump-nozzle combinations where the pump is able to provide the minimum nozzle supply pressure are shown. As is clear from Table III, there are no problems in reaching the minimum supply pressure for flat nozzle F, and all pumps except for P2 are able to reach sufficiently high pressures to ensure correct flowrate regulation in the circuit. With simple cone nozzles A and B, some critical conditions begin to arise, because the P2 pump is not able to guarantee the minimum pressure for correct operation. The situation worsens in the case of nozzle C, as only two pumps P4 and P5 can supply sufficient pressure. The worst situations are with the largest simple cone model, nozzle D, which can be supplied by only one of the selected pumps because of its large size, and with air induction cone nozzle E, the smallest in the catalog, as only one of the pumps can provide the higher minimum pressures required for this type.

Table III – Some simulations carried out with the various pumps

Pump	Nozzle	p nozzle (bar)	Tank emptying time (s)
P1	A	4.18	660
P3	A	3.70	695
P4	A	5.85	570
P5	A	6.03	560
P1	B	3.68	520
P3	B	3.21	555
P4	B	5.05	450
P5	B	5.70	425
P4	C	3.68	350
P5	C	5.02	300
P5	D	4.28	215
P5	E	5.01	300
P1	F	2.95	385
P2	F	1.39	560
P3	F	2.44	420
P4	F	3.67	350
P5	F	4.97	295

All configurations with these five pumps and six nozzles were tested with circuit 1. As simulation data shows, the 10-liter tank emptying time associated with each nozzle is an important factor. To optimize the spraying process, care must be taken to select a nozzle with which the tank is emptied in a time that matches drone battery life as closely as possible. Today's drones still have limited battery life—about 15 minutes at full load—so if the number of tank refilling operations is not optimized, time will be wasted in filling the tank and rechanging the batteries. In addition, batteries are very expensive and it is advisable to be able to make full use of the guaranteed battery life between charges. In circuit 1, the pump motors were operated at their maximum angular velocity. Consumption was determined using the sensor designated by the symbol ∫ Q, which measures the total volume of liquid pumped versus time. As the tank volume in this simulation was assumed to be 12 l, the instant when this sensor measures 10 l was used to determine tank emptying time. Various operating conditions were analyzed, as shown in Figures 8a-c.

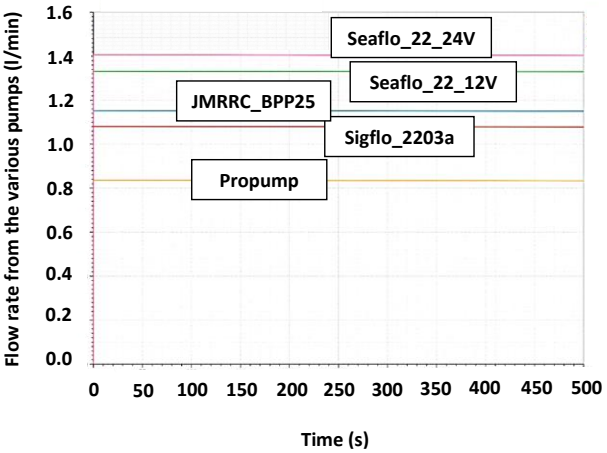

Figure 8a Flowrate from nozzle B with various pumps, pressures as shown in Figure 5.

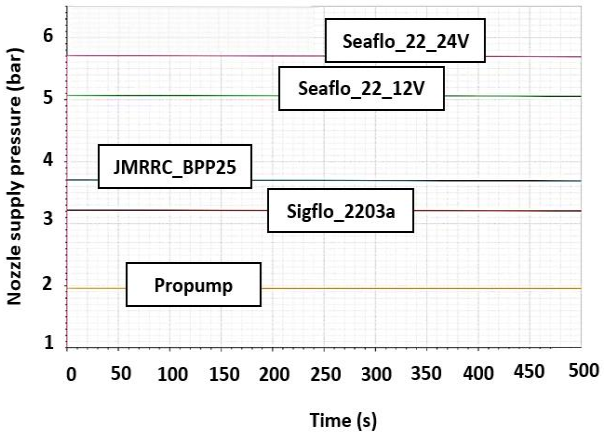

Figure 8b Nozzle B supply pressure with each pump.

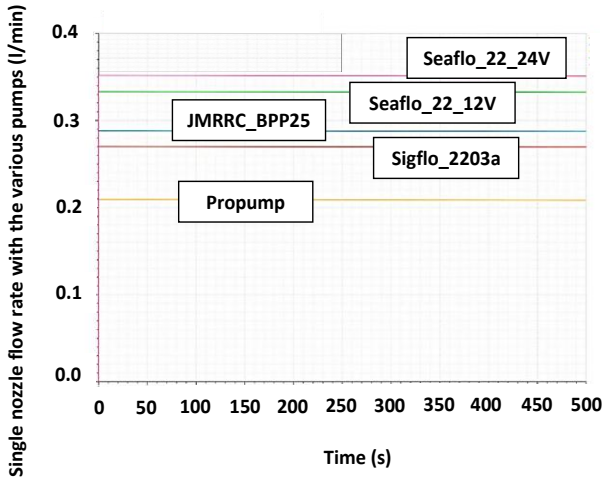

Figure 8c Flowrate in nozzle B with each pump.

Figure 8b was useful in determining the circuit's ability to supply the nozzles at constant pressure. Methods of taking full advantage of battery life and thus optimizing the entire process were discussed with several users of drones in agriculture. One suggestion was to make the first pass with 10 l in the tank, empty it in about 450 s, return the drone to the tank filling station, and then make the second pass emptying the tank about 240 s. In this way it is possible to spray for 12 minutes and have 3 minutes of residual battery life so that the drone can return without having to make an emergency landing. Liquid and powdered pesticides must be diluted with water before use. If dilution is insufficient, nozzle obstruction can occur because of the small fluid passage section, causing circuit malfunctions and irregular spraying. To investigate circuit behavior during partial or total nozzle obstruction, circuit 2 (Figure 9) was built on the simulation platform. This investigation is very important, because tubing or nozzle obstruction can cause a pressure increase which will damage the circuit, burst tubing and lead to dangerous drone instability. Circuit 2 is similar to the one in Figure 7, except that two flowmeters measuring the flowrate of the two circuit branches have been added and the nozzle designated as PN is a piloted nozzle in which the passage section can be progressively reduced via a variable signal. In circuit 1, pump was simulated using the manufacturer's specifications, the L and T connections were modeled in order to simulate pressure loss, the nozzles were simulated using the procedure described above, and simulation duration was set to approximately 500 s to simulate a real case where the tank is emptied and the drone batteries are exhausted. In circuit 2, the pump parameters and nozzles were modeled in the same way as in circuit 1, but using pump P5 and nozzle B. Simulation duration was here set to 180 s and the nozzle control signal simulating nozzle failure, was increased at 60 s intervals to investigate the condition with nozzle fully open, nozzle 50% obstructed, and nozzle fully obstructed. Thus, both the nozzle and the pump were used to simulate a failure scenario in circuit 2. In this circuit, the operator controls nozzle and pump by means of a signal varying over time. Simulation can take place in steps, in which control signal value and step duration can be established.

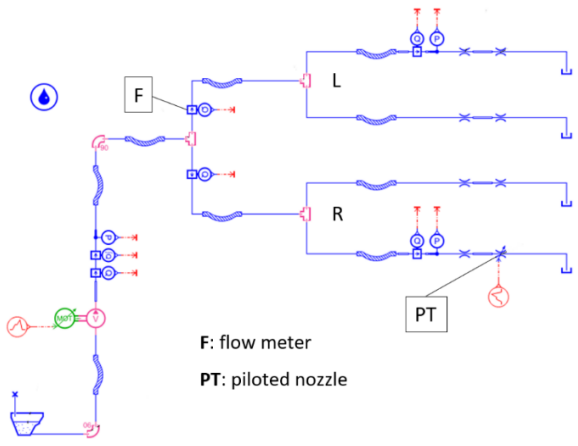

Figure 9 Circuit 2 used to simulate nozzle failure.

Nozzle obstruction is a problem that can occur easily, given the environment in which it operates. Even when filling the tank, foreign bodies can end up in the liquid and be pumped through the circuit. During flight, the pilot must focus on the flight path, rather than whether or not the nozzles are spraying well. It is thus advisable to have a system that identifies circuit malfunction and alerts the pilot with a warning signal. As the nozzle gradually clogs, pump outlet pressure tends to increase while overall flowrate tends to decrease.

As can be seen from Figure 10a, which shows liquid flowrate in the two branches as the nozzle clogs, the flowrate in the two branches tends to diverge as passage section is reduced. In fact, the flowrate decreases in branch R where failure occurs, and gradually increases in branch L that operates correctly. By positioning a flowmeter on each branch as shown in Figure 9, acquiring the analog flow data instant by instant, and comparing the data from the two flowmeters, an alarm signal can be generated to warn of impending circuit failure or malfunction. Some simulations carried out with circuit 2 are illustrated in Figures 10a and b. Figure 10a shows the simulated flowrate in the two circuit branches during nozzle failure, while Figure 10b shows the pressure increase due to nozzle failure, which can reach a level that damages the tubing in a part of the circuit, causing the drone to overturn. Such potential scenarios are interesting to analyze, and it is important that the models be able to simulate all conditions under which the spraying circuit operates correctly or fails.

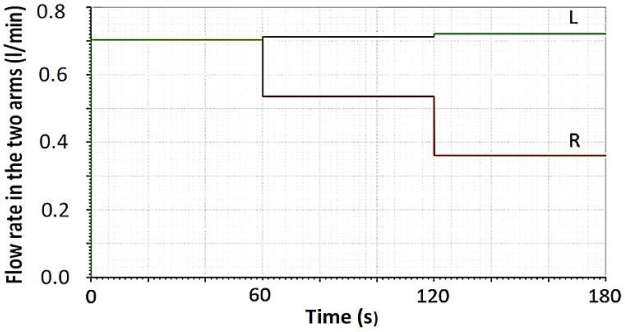

Figure 10a Liquid flowrate in the two branches of circuit 2 during nozzle failure.

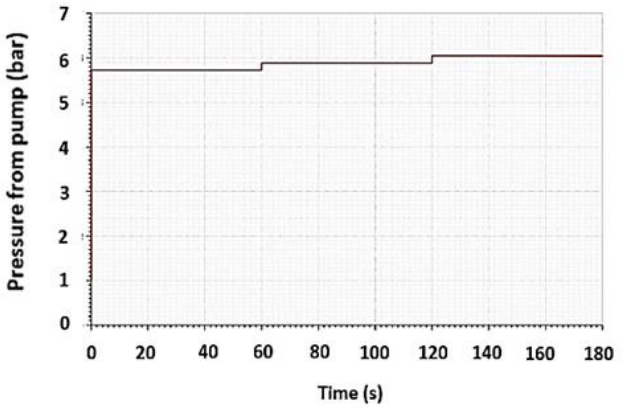

Figure 10b Pressure increase for nozzle failure.

7 THE SECOND PROPOSED NOZZLE MODELLING TECHNIQUE

The second technique for modeling the nozzle on the Simcenter Amesim platform was based on nozzle catalog data processed using commercial software (Microsoft Office Excel 2003) to obtain more information on nozzle pressure and flowrate and to plot a more accurate flowrate versus pressure curve. Microsoft Office Excel 2003 was then used to find the best polynomial expressions for modeling nozzle behavior. In this preliminary step, both the catalog data and the intensified catalog data were then uploaded onto the Simcenter Amesim platform to simulate the nozzles. In the future, the authors will conduct further simulations on the platform to improve the nozzle models. In all the graphs where polynomial expressions were presented x is referred to the abscissa axis, y is referred to the ordinate axis. The graphs in Figures 11a-d and Figures 12a-c show the nozzle characteristic and the polynomial expression used to simulate it for nozzle G (full cone jet) and nozzle M (flat jet). For these graphs authors underline: in orange the 5th (Figure 11a), the 3rd (Figure 11b), the 2nd (Figure 11c), the 6th (Figure 11d), the 5th (Figure 12a), the 4th (Figure 12b), the 3rd (Figure 12c) polynomial expression; in blue the catalogue data (intensified data). Figure 13a shows the best solution obtained for nozzle G, using 5th and 2nd order polynomial expressions, while Figure 13b shows the best solution for nozzle M, using 4th and 5th order polynomial expressions.

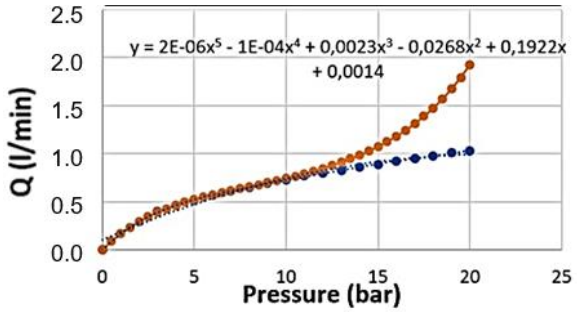

Figure 11a Flowrate versus pressure behavior from intensified catalog data with polynomial expressions (nozzle G).

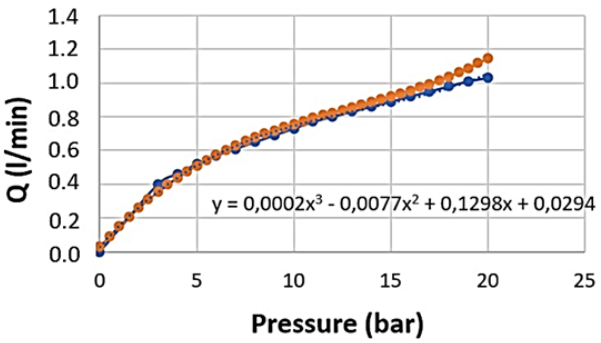

Figure 11b Flowrate versus pressure behavior from catalog data with additional polynomial expressions (nozzle G).

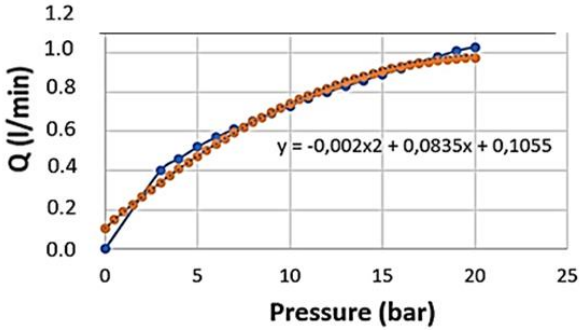

Figure 11c Flowrate versus pressure behavior from catalog data with additional polynomial expressions (nozzle G).

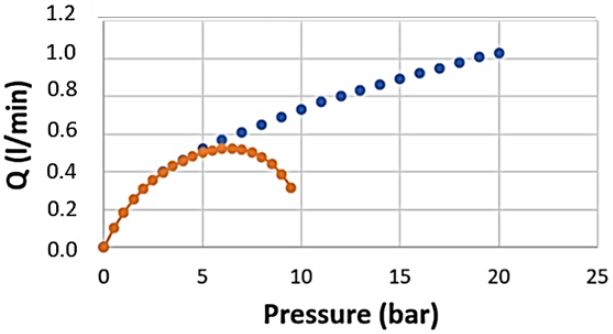

Figure 11d Flowrate versus pressure behavior from catalog data with additional polynomial expressions (nozzle G).

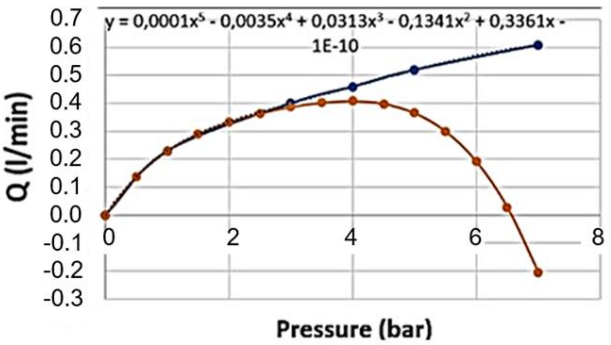

Figure 12a Flowrate versus pressure behavior from catalog data with polynomial expressions (nozzle M).

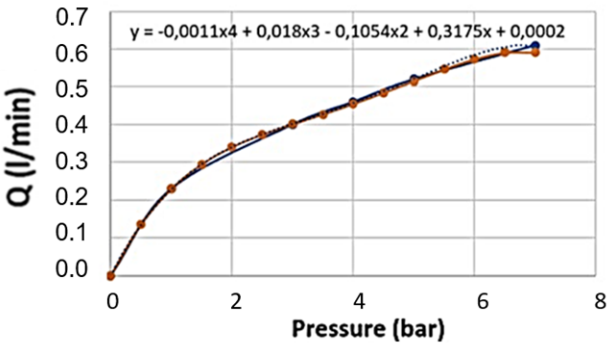

Figure 12b Flowrate versus pressure behavior from catalog data with additional polynomial expressions (nozzle M).

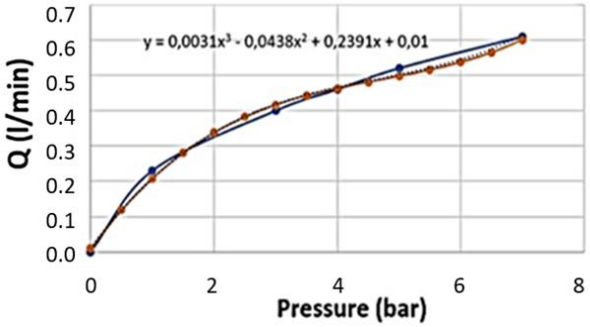

Figure 12c Flowrate versus pressure behavior from catalogue data with polynomial expressions (nozzle M).

Simulations were initially performed with one nozzle at a time (Figure 14), first with model G and then with model M. In this case especially the catalog intensified data model was used to simulate the nozzle. The four-nozzle circuit (Figure 15) was used to test these two nozzles in the following conditions: model G with catalog data; model G, with intensified catalog data; model M with catalog data; and model M with intensified catalog data. Results were satisfactory and demonstrate that this procedure can simulate nozzle behavior correctly. This simulation method on the Simcenter Amesim platform could be faster than the first proposed technique, and can reproduce the nozzle characteristic curve over a wider range of supply pressures.
In addition, it can zoom in on the details required in a specific area of the pressure range if the studied application calls for low or medium/high pressure levels.

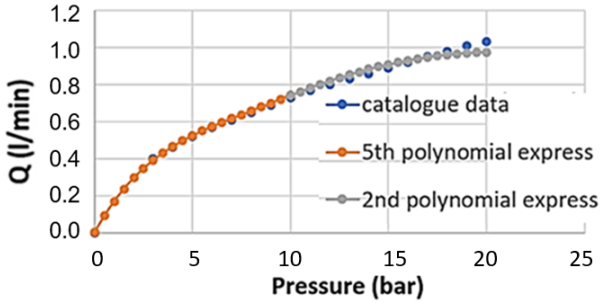

Figure 13a Flowrate versus pressure behavior from catalog data and selected polynomial expressions (nozzle G).

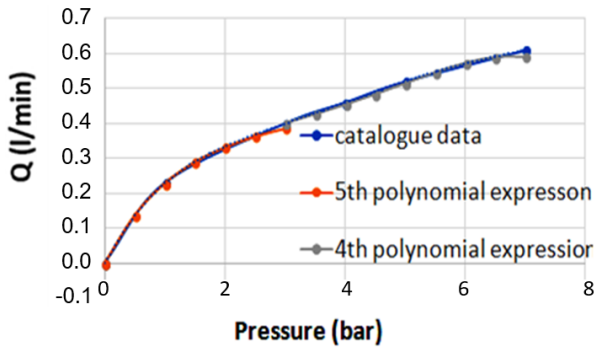

Figure 13b Flowrate versus pressure behavior from catalog data and selected polynomial expressions (nozzle M).

It was thus possible to find the polynomial expressions that best reproduce nozzle behavior.
Figure 14 shows the circuit used on the Simcenter Amesim platform to simulate a single nozzle with this second technique.

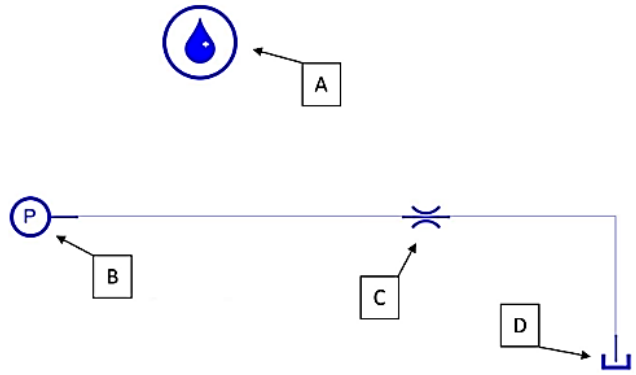

Figure 14 The single nozzle model produced with the second proposed technique.

The circuit consists of the elementary hydraulic properties section (A) used to set or modify all fluid properties during simulation; pressure source (B); flowcontrol-restrictor (C), which is the main circuit component and the main part to be modeled; and tank (D), which simulates the environment at atmosphere pressure where the pesticide is sprayed. A simplified four-nozzle sprayer circuit is illustrated in Figure 15.In this case the circuit was modeled to simulate nozzle behavior, rather than the entire circuit as in the previous simulation shown in Figure 7. Nozzle operation during the simulation was verified by using the intensified catalog data on the software platform. With both a single nozzle and with four nozzles, nozzle flowrate versus time as shown in Figures 16a and b was in line with the characteristic curve obtained using catalog data (Figures 11a-d and Figures 12a-c). This demonstrates the models' reliability.

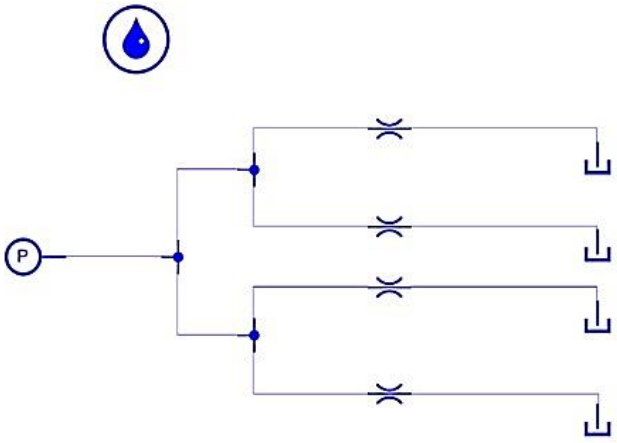

Figure 15 An example of the four-nozzle sprayer circuit model.

8 COMMENTS ON RESULTS

After analyzing several nozzles and commercial pumps, we will now turn to the use of the drone in the vineyard. With simple cone and air induction cone nozzles, criticalities arise because these units require high supply pressures which make it necessary to use a high performance pump with non-negligible weight. Figures 16a and b and Figures 16c and d show some results obtained from the simulation with the single-nozzle circuit and with the four-nozzle circuit respectively. Unlike flat nozzles that can also work well with pump P1, air induction nozzles require pump P5, which weighs about 0.8 kg. This is a significant increase for drone applications.

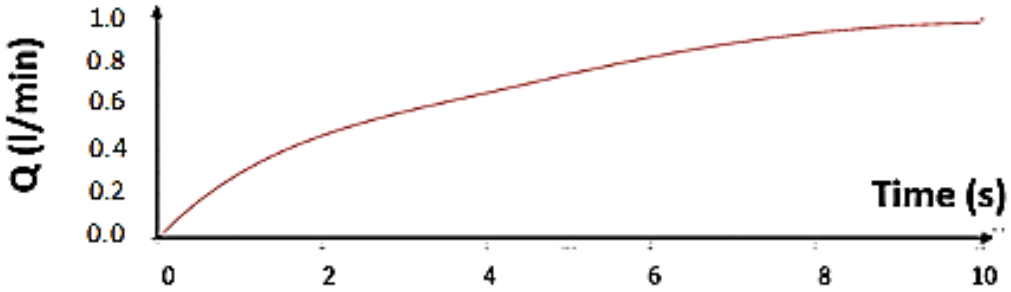

Figure 16a Flowrate versus time obtained from the simulation with the circuit shown in Figure 14 and nozzle G.

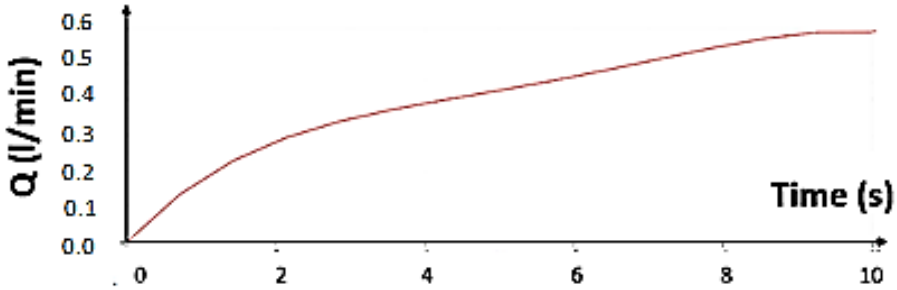

Figure 16b Flowrate versus time obtained from the simulation with the circuit shown in Figure 14 and nozzle M.

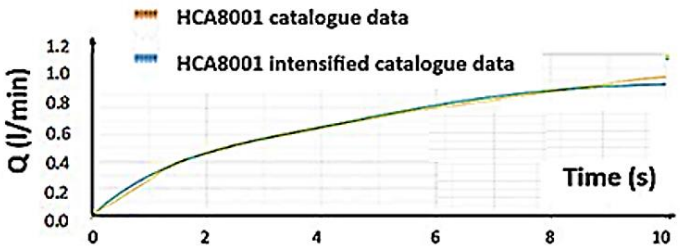

Figure 16c Flowrate versus time obtained from the simulation with the circuit shown in Figure 15 and nozzle G, comparing catalog data and intensified catalog data.

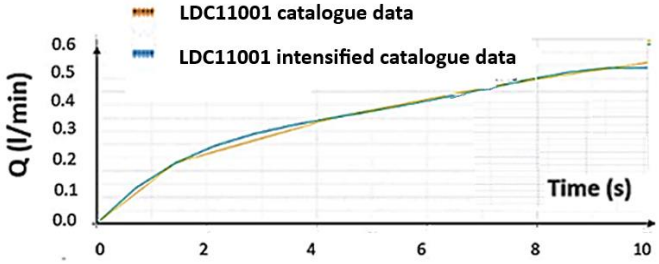

Figure 16d Flowrate versus time obtained from the simulation with the circuit shown in Figure 15 and nozzle M, comparing catalog data and intensified catalog data.

In addition to ensuring that nozzles operate correctly, particular attention must be given to selecting the appropriate nozzle size, as most nozzles on the market are designed for use on tractor-towed sprayers and thus to deliver large amounts. In such conventional spraying operations, in fact, hundreds of liters of water are used per hectare of cultivation. The high flowrates delivered by these nozzles can be a problem. To be beneficial, drones must spray 40-50 liters per hectare of crop, and using nozzles like E will empty the tank too quickly, necessitating frequent, time-consuming refills. As for nozzle clogging, which is a concrete and rather common problem, it is advisable to clean nozzles frequently and provide a system such as the one discussed above to warn the pilot of impending failure. When the second technique was used to model the nozzles, the circuit simulation yielded good results. We can thus conclude that both techniques presented here model each model correctly.

9 SOME PRELIMINARY EXPERIMENTAL TESTS

Authors carried out in the DIMEAS Laboratory Department (Politecnico di Torino) a lot of experimental tests using a specific vineyard simulator and photographic paper to analyze the sprayed jets. Tests were carried out with practically all available Arag Group ASJ Spray-Jet nozzles. Some of these experimental tests were conducted with the circuit shown in Figures 17a, 17b, 17c. In particular Figure 17b shows the details and the position of the three nozzles (indicated by the yellow circles) in comparison with the paper simulating the vineyard. This circuit was not till now connected under a drone, looking anyway for future experimental tests in the open environment using the best circuit configuration individuated through all this study.

Figure 17a Circuit used for laboratory tests, supplied by a pressurized tank.

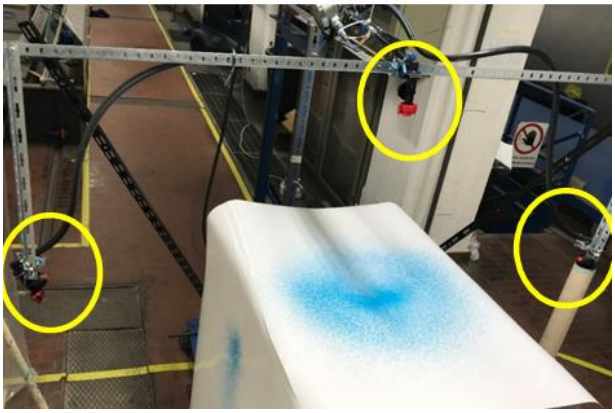

Figure 17b Some details of the three nozzles used and of the paper simulating the vineyard.

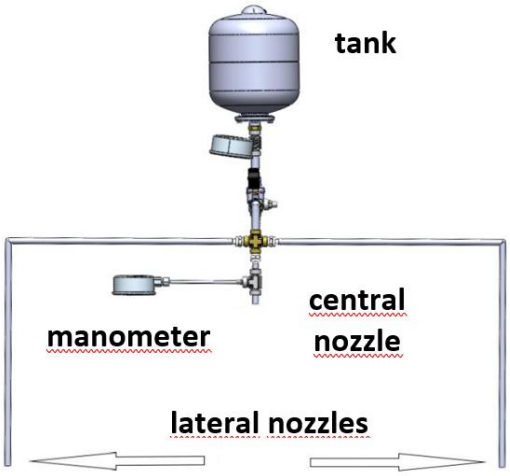

Figure 17c Experimental circuit layout.

In all the tests here illustrated the nozzles were in a stationary condition. Here a pressurized tank was connected to the optimized spraying circuit, consisting of three nozzles (e.g., one central full jet cone nozzle H; two lateral flat jet nozzles M). Numerous experimental tests were conducted in which the circuit's liquid consumption was also investigated.
On average, the tank was completely emptied after 174 s, starting from a volume of 5 l, 4 bar tank pressure and 2.5 bar nozzle supply pressure. Under these conditions, experimental flowrate (i.e., the circuit's liquid consumption) was 0.57 l/min for each nozzle. Some of these experimental tests were used to compare the real and simulated liquid consumption to check nozzle reliability. Using the first nozzle simulation technique (as shown in Figure 18) with full cone nozzle B supplied at 2.75 bar, the maximum calculated flowrate was 0.28 l/min, while the flowrate stated in the catalog was 0.25 l/min at the same supply pressure. The flowrates shown in Figure 8c for this nozzle with each pump vary from 0.23 l/min to 0.36 l/min.

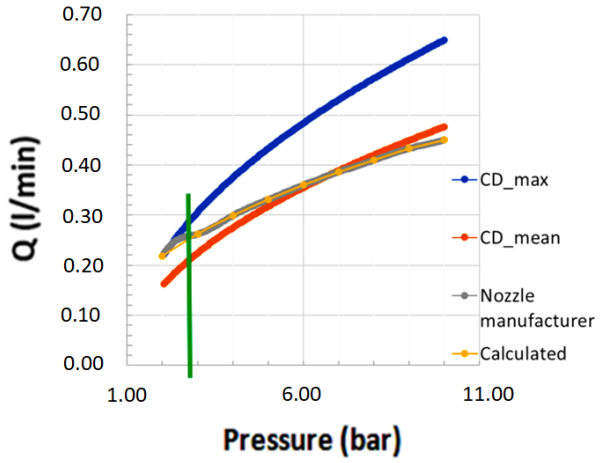

Figure 18 Flowrate versus pressure for full cone nozzle B.

The flowrate calculated from intensified catalog data for nozzle G supplied at 2.5 bar was about 0.38 l/min as shown in Figure 19a, while the flowrate calculated from intensified catalog data for nozzle M supplied at 2.5 bar was also about 0.38 l/min as shown in Figure 19b. These flowrates were a little lower than the those based on the nozzle catalog data which were used for the simulations, but this preliminary comparison between the simulated and experimental data is useful for validating the procedure employed in design the nozzle models. If catalog data is used for these nozzles, flowrate is 0.77 l/min for nozzle G at 5 bar and 0.40 l/min for nozzle M at 3 bar.

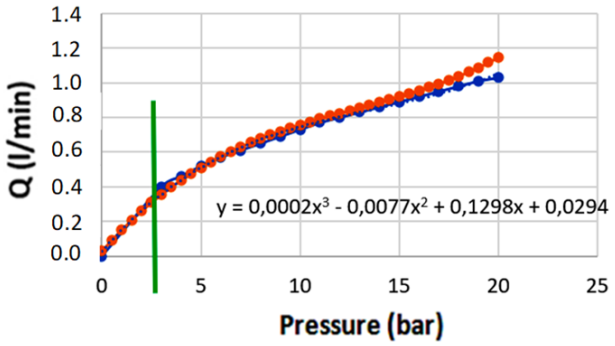

Figure 19a Flowrate versus pressure in nozzle G (orange: 3rd polynomial expression; blue: intensified catalog data).

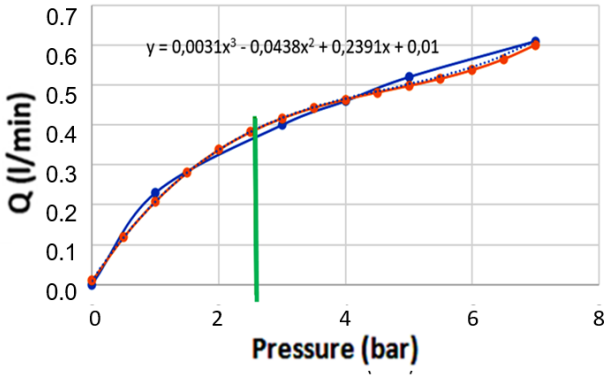

Figure 19b Flowrate versus pressure in nozzle M (orange: 3rd polynomial expression: blue: intensified catalog data).

The catalog data and the data used on the Simcenter Amesim platform differed somewhat from the experimental results from some preliminary tests.

In any case, we can say that the second nozzle modeling technique makes it possible to simulate any model of sprayer nozzle, to investigate its characteristics both alone or in a sprayer circuit and to optimize the design of the entire spraying system. Both the procedures illustrated here for simulating nozzle behavior starting from catalog data yield good results and can produce useful models for circuit simulation and design. In particular considering an average flowrate from the catalog or from the nozzle modelling results about 0,60 l/min, the percentage error with the experimental nozzle flowrate equal to 0,57 l/min was about 5,4 %.

10 CONCLUSIONS

This paper illustrated several models of agricultural nozzles for use on a drone-mounted vineyard spraying circuit developed on a commercial software platform. The investigation started with an analysis of vineyard characteristics and a number of commercial nozzles that can be used for this application. After identifying appropriate drone flight paths in the vineyard, commercial nozzles were selected for a preliminary spraying circuit layout. A procedure was developed for modeling these nozzles on a commercial software platform which was then used to simulate their operation. Two nozzle modeling techniques were presented: one using coefficients calculated from the literature, and another using catalog data and mathematical expressions to describe and simulate nozzle operation. Both techniques yielded good results, enabling the entire spraying circuit to be reproduced on the commercial software platform. Results from the second nozzle modeling technique were then compared with nozzle catalog data, again yielding good results. Operation was thus investigated under a variety of conditions and drone flight parameters.

The procedure allows to have an interesting tool to study, to design and to test different kinds of spraying circuits. It can improve all the design process of these circuits, avoiding the need of numerous experimental tests before to individuate the optimum configuration and components. The study was original and can provide a basis for future work on nozzles and other circuit components, improving the selection process. In particular, using the models constructed on the software platform together with experimental tests, the CAD vineyard model, nozzle specifications and studies of the nozzles directly in CAD vineyard model can provide useful information on pesticide consumption, optimum drone flight strategies, and crop coverage obtained with different nozzle types, number and layout on the drone. As future experimental tests will also be carried out with an anti-sloshing tank which prevents liquid motion when the drone is in flight, the circuit models on the software platform will be improved to simulate this kind of tank.

11 ACKNOWLEDGEMENTS

This study was funded by MIUR, the Italian Ministry for Education, Universities and Research, as part of PRIN Project 2017 “New technical and operative solutions for the use of drones in Agriculture 4.0”.
Authors thank the engineers T.F. Bianchet, D. Caroppo, A. Conte, A. Frate, P. Gala, M. Persico and L. Vaudano for their help in this study.
The authors thank the M. Martinelli family, owners of the “Antica Meridiana Relais-Art” Dolcetto vineyard in Vicoforte (CN) Italy and the Massimo Pastoris family, owners of the Azienda Agricola Pastoris vineyard in Viverone (BI) Italy for their help in providing crop dimensions.

REFERENCES

[1] Diaconu A., Tenu I., Rosca R. and Cârlescu P., Researches regarding the reduction of pesticide soil pollution in vineyards. *Process Safety and Environmental Protection*, Vol. 108, pg. 135-143, 2017.

[2] Mogili U.M.R. and Deepak B.B.V.L., Review on Application of Drone Systems in Precision Agriculture. *Procedia Computer Science*, Vol. 133, pp. 502-509, 2018.

[3] Vallet A., Tinet C. and Douzals J.P., Effect of nozzle orientation on droplet size and droplet velocity from vineyard sprays. *Journal of Agricultural Science and Technology (JAST)*, Vol. 5, pp. 672-678, 2015.

[4] Chen S., Lan Y., Zhou Z., Ouyang F., Wang G., Huang X., Deng X. and Cheng S., Effect of Droplet Size Parameters on Droplet Deposition and Drift of Aerial Spraying by Using Plant Protection UAV. *Agronomy 2020 MDPI*, Vol. 10, No. 2, pp.195-210, 2020.

[5] Guo Q., Zhu Y., Tang Y., Hou C., He Y., Zhuang J., Zheng Y. and Luo S., CFD simulation and experimental verification of the spatial and temporal distributions of the downwash airflow of a quad-rotor agricultural UAV in hover. *Computers and Electronics in Agriculture*, Vol. 172, May 2020, 105343, 2020.

[6] Wen S., Hanb J., Ning Z., Lan Y., Yin X., Zhang J. and Ge Y., Numerical analysis and validation of spray distributions disturbed by quadrotor drone wake at different flight speeds, *Computers and Electronics in Agriculture*, Vol. 166, Issue C, 105036, 2019.

[7] Sehsah E.M.E. and Ganzelmeier H., Comparison study on low pressure EMTF nozzles based on droplets size characteristics. *Misr J. Ag. Eng. Farm Machinery and Power*, Vol. 27, No. 1, pp. 122-140, 2010.

[8] Srivastava A.K., Goering C.E., Rohrbach R.P. and Buckmaster D.R., Engineering Principles of Agricultural Machines. *American Society of Agricultural Engineers*, Vol. 631, S774, 1993.

[9] Yu S.H., Kim Y.K., Jun H.J., Choi I.S., Woo J.K., Kim Y.H., Yun Y.T., Choi Y., Alidoost R. and Lee J., Evaluation of Spray Characteristics of Pesticide Injection System in Agricultural Drones. *Journal of Biosystems Engineering*, Vol. 45, pp. 272-280, 2020.

[10] Gong J., Fan W. and Peng J., Application analysis of hydraulic nozzle and rotary atomization sprayer on plant protection UAV. *Int. J. Precis. Agric, Aviat*, Vol. 2, No.1, pp. 26-30, 2019.

[11] Karan K.S. and Vimalkumar R., Design and Development of a Drone for Spraying Pesticides, Fertilizers and Disinfectants. *International Journal of Engineering Research & Technology (IJERT)*, Vol. 9, Issue 05, pp. 1181-1185, 2020.

[12] Faiçal B.S., Freitas H., Gomes P.H., Mano L.Y., Pessin G., de Carvalho A.C.P.L.F., Krishnamachari B. and Ueyama J., An adaptive approach for UAV-based pesticide spraying in dynamic environments. *Computers and Electronics in Agriculture*, Vol. 138, pp. 210-223, 2017.

[13] Ling W., Du C., Mengchao Z., Yu W., Ze Y. and Shumao W., CFD Simulation of Low-attitude Droplets Deposition Characteristics for UAV based on Multi-feature Fusion. *IFAC-PapersOn line*, Vol. 51, Issue 17, pp. 648-653, 2018.

[14] Zhang H., Qi L., Wu Y., Musiu E.M., Zhenzhen Cheng Z. and Wang P., Numerical simulation of airflow field from a six-rotor plant protection drone using lattice Boltzmann method. *Biosystems Engineering*, Vol. 197, pp. 366-351, 2020.

[15] Talaviya T., Shah D., Patel N., Yagnik H. and Shah M., Implementation of artificial intelligence in agriculture for optimisation of irrigation and application of pesticides and herbicides. *Artificial Intelligence in Agriculture*, Vol. 4, pp.58-73, 2020.

[16] Fornasiero D., Mori N., Tirello P., Pozzebon A., Duso C., Tescari E., Bradascio R. and Otto S., Effect of spray drift reduction techniques on pests and predatory mites in orchards and vineyards. *Crop Protection*, Vol. 98, pp. 283-292, 2017.

[17] Guo S., Li J., Yao W., Zhan Y., Li Y. and Shi Y., Distribution characteristics on droplet deposition of wind field vortex formed by multi-rotor UAV. 2019, *PLoS One*, Vol. 14, No. 7, e0220024, 2019.

[18] Al Heidary M., Douzals J.P., Sinfort C. and Vallet A., Influence of spray characteristics on potential spray drift of field crop sprayers: A literature review. *Crop Protection*, Vol. 63, pp.120-130, 2014.

[19] Gan-Mor S., Ronen B. and Ohaliav K., The effect of air velocity and proximity on the charging of sprays from conventional hydraulic nozzles. *Biosystems Engineering*, Vol. 121, pp.200-208, 2014.

[20] Belforte G., Eula G. and Raparelli T., Innovative Prototype For Automatic Pesticide Spraying in Greenhouses. *Conference RAAD08*, Ancona (Italy), September 2008, pp. 15-17, 2008.

[21] Belforte G., Eula G. and Raparelli T., Analysis of Pneumatic Techniques for Pesticide Spraying in Greenhouses. *Experimental Techniques*,

November/December 2009, Vol. 33, Issue 6, pp. 21-29, 2009.

[22] Belforte G., Eula G. and Raparelli T., DeVoPeS: Defined Volume Pesticide Sprayer design and testing. *Experimental Techniques*, November/December 2011, Issue of Experimental Techniques, Vol. 35, No. 6, pp.14-26, 2011.

[23] Belforte G., Eula G. and Raparelli T., *A new technique for safe pesticide spraying in greenhouses*. Chapter 8 in Pesticides: formulations, effects, fate. Intechweb, Ed. Margarita Stoytcheva, January 2011, pp.129-154, 2011.

[24] Belforte G. and Eula G., Smart pneutronic equipments and systems for mechatronic applications. *Journal of Control Engineering and Applied Informatics*, CEAI, Vol. 14, No. 4, pp. 70-79, 2012.

[25] Raparelli T., Eula G., Ivanov A. and Pepe G., Project of An Experimental Simulator Designed To Analyse Pesticide Spraying Techniques In Vineyard Using Drones. *International Journal of Mechatronics and Applied Mechanics*, Vol. 1. Issue 10, pp. 64-71, 2021.

[26] Eula G., Fiori R. and Goti E., A preliminary proposal for characterizing leaves to improve pesticide spraying in the open field. *JoMac International Journal of Mechanics and Control*, Vol. 24, No. 1, pp. 107-124, 2023.

[27] Pásztor J., Kakucs A., Timár Z. and Egyed-Faluvégi E., Droplet size analysis of spray nozzles. *Papers on Technical Science*, Vol. 12, pp. 62-66, 2020.

[28] Raparelli T., Ivanov A. and Eula G., Pesticide spraying systems for vineyards using drones. Submitted to *JoMac International Journal of Mechanics and Control*, on 18th May 2023 (in progress, pending review).

[29] Teejet Technologies catalogue available on www.teejet.com.

[30] ASJ Spray-jet ARAG Group asjnozzle.it/.

International Journal of Mechanics and Control – JoMaC
Published by ASTRA M B S.R.L.

TRANSFER OF COPYRIGHT AGREEMENT

NOTE: Authors/copyright holders are asked to complete this form signing section A, B or C and mail it to the editor office with the manuscript or as soon afterwards as possible.	*Editorial Secretary address:* Andrea Manuello Bertetto Matteo D. L. Dalla Vedova, Simone Venturini, Alessandro Aimasso *Dept. of Mechanical and Aerospace Engineering* *Politecnico di Torino* *C.so Duca degli Abruzzi, 24 – 10129 Torino – Italy* *e_mail: jomac@polito.it* *fax n.: +39.011.090.6999*

The article title:

By:_____

To be Published in ***International Journal of Mechanics and Control JoMaC***
Official legal Turin court registration Number 5320 (5 May 2000) - reg. Tribunale di Torino N. 5390 del 5 maggio 2000

A Copyright to the above article is hereby transferred to the JoMaC, effective upon acceptance for publication. However the following rights are reserved by the author(s)/copyright holder(s):
1. All proprietary rights other than copyright, such as patent rights;
2. The right to use, free or charge, all or part of this article in future works of their own, such as books and lectures;
3. The right to reproduce the article for their own purposes provided the copies are not offered for sale.

To be signed below by all authors or, if signed by only one author on behalf of all co-authors, the statement A2 below must be signed.

A1. All authors:

SIGNATURE_____DATE_____ SIGNATURE_____DATE_____

PRINTED NAME_____ PRINTED NAME_____

SIGNATURE_____DATE_____ SIGNATURE_____DATE_____

PRINTED NAME_____ PRINTED NAME_____

A2. One author on behalf of all co-authors:
"I represent and warrant that I am authorised to execute this transfer of copyright on behalf of all the authors of the article referred to above"

PRINTED NAME_____

SIGNATURE_____ TITLE_____ DATE_____

B. The above article was written as part of duties as an employee or otherwise as a work made for hire. As an authorised representative of the employer or other proprietor. I hereby transfer copyright to the above article to *International Journal of Mechanics and Control* effective upon publication. However, the following rights are reserved:
1. All proprietary rights other than copyright, such as patent rights;
2. The right to use, free or charge, all or part of this article in future works of their own, such as books and lectures;
3. The right to reproduce the article for their own purposes provided the copies are not offered for sale.

PRINTED NAME_____

SIGNATURE_____ TITLE_____ DATE_____

C. I certify that the above article has been written in the course of employment by the United States Government so that no copyright exists, or by the United Kingdom Government (Crown Copyright), thus there is no transfer of copyright.

PRINTED NAME_____

SIGNATURE_____ TITLE_____ DATE_____

CONTENTS - Special Issue of the International Journal of Mechanics and Control (JoMaC) dedicated to the 6th International Tunisian Conf. on Mechanics (COTUME 2023)

CONTENTS – Regular Issue

NEWS FROM THE JOMAC EDITORIAL BOARD:

Starting from the June 2024 issue, JoMaC provides an Open Access service to our authors. You are invited to visit the JoMaC website (http://www.jomac.it) for further details.